Chemical Engineering Journal 455 (2023) 140765

Contents lists available at ScienceDirect

Chemical Engineering Journal

journal homepage: www.elsevier.com/locate/cej

Aquivion-based anion exchange membranes: Synthesis optimization via dispersant agents and reaction time

Alessandra Carbone [a,*], Sabrina Campagna Zignani [a], Irene Gatto [a], Rolando Pedicini [a], Claudio Oldani [b], Alice Cattaneo [b], Antonino Salvatore Aricò [a]

[a] CNR-ITAE, via S. Lucia sopra Contesse, 5, Messina, Italy
[b] Solvay Specialty Polymers, Viale Lombardia 20, 20021 Bollate, (MI), Italy

ARTICLE INFO

Keywords:
Anion exchange membranes
Quaternary ammonium
Aquivion®
Anion Conductivity
Anion exchange membrane water electrolysis

ABSTRACT

Alkaline membrane water electrolysis fed by renewable energy is a promising technology to produce "green" hydrogen for a variety of applications. Thanks to their unique characteristics of chemical, thermal and electrochemical stability, perfluorinated polymers are proposed as an alternative to hydrocarbon-based anion exchange membranes (AEMs) for applications in water electrolysers. A simple two-step functionalization reaction to introduce quaternary ammonium groups onto Aquivion® perfuorinated backbone is reported using a low toxicity dispersant. The most appropriate dispersant (Novec 7500) and reaction parameters (5 °C for 2 hrs) are selected. The complete conversion of the precursors into a quaternary ammonium salt is confirmed by a solid-state NMR study. Physico-chemical properties, thermal behavior and anion conductivity of the formed AEM are investigated. The phase separation characteristics of this perfluorinated polymer allow to reach a membrane ion mobility (μ_{eff}) 1.99 10^{-4} cm^2 V^{-1} s^{-1}, one order of magnitude higher than the FAA3-50 commercial membrane, meaning an enhanced ion dissociation. A very limited degradation of functional groups is demonstrated after immersion in alkaline solution, with only 2 % of ion exchange capacity (IEC) reduction against 14 % of the FAA3-50 commercial membrane. An electrolysis current density of 0.9 A cm^{-2} at 2.2 V and 90 °C, is achieved showing very promising applications for green hydrogen production.

1. Introduction

The large-scale production of energy from renewable sources will greatly contribute to the implementation of the objectives of the European energy policy, i.e. obtaining a 40 % reduction in greenhouse gas emissions, increasing renewable energies to 32 % and achieving energy savings of approximately 32.5 % by 2030 with the long-term goal of a climate-neutral Europe in 2050 [1]. However, due to the intermittent nature of renewable energy production, an innovative energy storage system is needed to provide a solution for an efficient use of renewable sources. The electrolysis of water using renewable energy is the most advanced technology for the production of "green" hydrogen for a variety of applications including transport, heat and electricity production and industrial uses. The electrolysis systems that are best coupled to renewable sources are solid state electrolysers with ion exchange membranes. In this context, the research is making great efforts to reach a sufficiently mature technology for market penetration [2]. The most used alkaline water electrolysis systems are, generally, based on porous diaphragm separators and concentrated liquid alkaline electrolytes, leading to high corrosion of the electrolyser components. To avoid this problem, continuous efforts are addressed to the development of components based on anion exchange membrane and electrocatalysts aiming at good performance and durability [3–23]. AEMs must meet the requirements of good anion conductivity, proper thermal, chemical and mechanical stability as well as high electrochemical stability in alkaline environment. Moreover, AEMs should be easy to process, and need to be produced by sustainable processes.[24] AEMs are generally based on polyaromatic or polyaliphatic backbone such as, among the others, polysulfone, poly(ether ketone), poly(phenylene oxide), fluorinated, polybenzimidazole, polyethylene, polystyrene, polyethylenepyrrole- co-polyethyleneketone, polyarylen piperidinium [25–30], with functional groups suitable for the ionic transport such as quaternary ammonium, imidazolium, pyridinium, benzimidazolium, piperidinum. [27,28,31–36]. All these membranes provide a good anion conductivity

* Corresponding author.
E-mail address: alessandra.carbone@itae.cnr.it (A. Carbone).

https://doi.org/10.1016/j.cej.2022.140765
Received 25 July 2022; Received in revised form 29 November 2022; Accepted 30 November 2022
Available online 2 December 2022

but, due to their polymeric backbone structure, they suffer of a poor chemical stability in alkaline environment, high swelling level and low durability [37–39]. Moreover, a trade-off between the mechanical strength and ionic conductivity should be considered for a good performance and stability.

To date, there is not a commercial reference adopted by the whole scientific community in this field, but different commercial membranes are used for this purpose. Generally, the commercial products are aimed to a broader field of applications such as electrolysis, fuel cells, electrodialysis, desalination, batteries [40–43]. Few commercial membranes are widely available such as Fumasep® (by Fumatech), Aemion® (by Ionomr), Sustainion® (by Dioxide Materials), Orion TM1 Durion™ (by Orion Polymer) and DURAION (by Evonik Industries AG) [44]. Interesting electrolysis results have been recently obtained with the PiperIon membrane (by Versogen) based on piperidinium functional group [24,26,45–50] showing current densities of 2.3 A cm^{-2} at 1.8 V at 80 °C.

Unfortunately, the high production cost and the low production scale makes some highly performing commercial membranes not yet mature for a large market penetration. In addition, it is not yet clear the durability of such AEMs in a practical electrolyser system. [24] In general, the performances, reported in the literature are referred to synthesized and commercial membranes operating at a temperature not exceeding 80 °C. A few papers report the electrolysis performance at 90 °C. A Membrane Electrode Assembly (MEA) containing a reinforced Fumatech FAA-3-PK-75 achieved 1 A cm^{-2} at 1.8 V using Pt/C and IrO_2 as an electrocatalysts. [51] Another paper [47] reports a promising performance of PAP-TP-85 achieving 1 A cm^{-2} at 1.8 V using Pt/C and Fe_x-Ni_yOOH-20F as electrocatalysts, however using large catalyst loading.

Only few papers report the use of perfluorinated polymers as anion exchange membranes even if there is a growing interest exploring this class of solid polyelectrolytes [52–55]. In particular, the modification of perfluorinated polymer precursors and membranes can allow to obtain AEMs with proper ion conductivity for application in alkaline electrochemical devices. The typical perfluorinated polymer structure, widely studied in acidic environment, induces a hydrophobic/hydrophilic phase separation aiming a good ion conductivity, reduced swelling and improved alkaline stability [25,56]. These properties make such kind of polymer attracting also in alkaline environment.

Thanks to their unique characteristics of chemical, thermal and electrochemical stability, perfluorinated polymers are proposed as an alternative to hydrocarbon-based anion exchange membranes (AEMs) for applications in water electrolysers. In this work, we report a simple two-step functionalization reaction, using low toxicity dispersing agents, to introduce quaternary ammonium groups onto the perfluorinated Aquivion® backbone. A good stability in alkaline environment was achieved after optimizing dispersant, temperature and reaction time. Limited degradation of functional groups was demonstrated after immersion in alkaline solution, with only 2 % of IEC reduction. Appropriate physico-chemical characteristics were observed for operation at 90 °C, in particular low swelling and stable anion conductivity was obtained. High temperature operation can strongly enhance reaction kinetics thus reducing the content of precursors or expensive electrocatalyst. Very promising water electrolysis performance was reached at 90 °C for this novel AEM, with a current density of 0.9 A cm^{-2} at 2.2 V at 90 °C with a voltage efficiency of about 70 %.

2. Materials and methods

2.1. Polymer synthesis and characterizations

2.1.1. Amidation reaction

Aquivion-SO_2F® (Solvay specialty polymers) with 720 g eq^{-1} EW (nominal IEC: 1.39 meq g^{-1}) was selected for the amidation reaction, whereas *N,N*,2,2-tetramethyl-1,3-propanediamine (Aldrich) was chosen as a diamine; DMSO (Aldrich), Ethanol (Carlo Erba) and NOVEC 7500 (3M™) were used as dispersants. After a preliminary study, the reaction temperature was set at 5 °C and different reaction times were investigated, in the range 30 min. −20 hrs.

An amount of 10 g of polymer was added under N_2 flow to the dispersant to have a 5 wt% dispersion. The dispersion was maintained at 5 °C for 2 hrs and then the *N,N*,2,2-tetramethyl-1,3-propanediamine was added drop by drop to react with the sulfonyl fluoride group. Three different reaction times: 30 min., 2 hrs and 20 hrs were considered. The obtained polymer was filtered, washed for 1 h in the same dispersing agent used for the reaction and collected by filtration. A washing step in KOH (Carlo Erba) 5 wt% solution for 1 h was carried out. Finally, the collected polymer was washed with 100 g ethanol twice for 30 min each. The polymer was filtered and dried in an oven at 70 °C under vacuum (1000 mbar) for 4 hrs.

2.1.2. Alkyation reaction

For the alkylation reaction, methyl tosylate (Alfa Aesar) was used as an alkylating agent. An amount of 5 g of dried amidated polymer was dispersed in anhydrous acetonitrile (Merck) at room temperature and mechanical stirred for 1 h, under N_2 flow. Then the reaction temperature was increased up to 50 °C and a stoichiometric amount of methyl tosylate, useful to convert all the amidated groups into alkylated ones, was added and left to react for 20 hrs. After cooling, the polymer was collected by means of a filtration and washed with acetonitrile for 30 min. Afterwards, 3 washing steps in ethanol, of 30 min each, were carried out and the polymer was dried at 70 °C under vacuum for 4 hrs.

2.2. Membrane preparation

The alkylated polymer was dispersed in dimethylacetamide (DMAc-Aldrich) at 80 °C under stirring for 4 hrs, thereafter centrifuged and separated from the solid part. The clear solution (5 wt%) was placed in a Petri dish and dried at 80 °C for 3 hrs. The membranes were detached from the Petri dish by dipping in water and left to dry between filter papers and thereafter thermally treated at 200 °C for 30 min to improve the mechanical properties. The quaternized membrane with tosylate counter-ions was exchanged for 72 hrs at room temperature in NaCl (Aldrich) 1 M solution to exchange the tosylate with chloride ions.

2.3. Ion exchange capacity measurements

2.3.1. Polymer acid-base titration

The acid-base back-titration of amidated polymer was carried out by in dispersing 0.3 g in 50 ml of isopropanol (Acros) and 8 ml of HCl 0.1 M (Carlo Erba). The dispersion was stirred at room temperature for 4 hrs and then water was added to reach 100 ml. The polymer was left to settle on the bottom of the beaker and 50 ml of the clear solution on the top was taken, added to 20 ml of distilled water and the excess of acid was titrated with NaOH 0.1 M (Carlo Erba).

The IEC was calculated as follows (Eq. (1)):

$$IEC = \left(V_i - V_{ep}\right)*[NaOH]/m_{dry} \quad (1)$$

Where:

V_i is the initial volume, expressed in ml.

V_{ep} is the volume of the titrant at the equivalent point expressed in ml.

[NaOH] is the concentration of titrant, expressed in molarity.

m_{dry} is the dry mass in grams of the sample determined at 70 °C for 2 hrs under vacuum (1000 mbar).

2.3.2. Membrane acid-base titration

The quaternized membrane acid-base back-titration was carried out by immersing the dried sample in hydro-alcoholic (water/ethanol 1:1 vol) KOH 1 M solution at room temperature for 24 hrs, then taking away the membrane from the solution and washing to remove the excess of

hydroxide ions. Successively, the membrane was immersed in HCl 0.1 M for 24 hrs at room T, then it was removed from the solution and back-titred with NaOH 0.1 M.

The IEC was calculated as follows in Eq. (2):

$$IEC = (V_{HCl} - V_{NaOH})*[NaOH]/m_{dry} \quad (2)$$

Where:

V_{HCl} is the initial volume, expressed in ml.

V_{NaOH} is the volume of the titrant at the equivalent point expressed in ml.

[NaOH] is the concentration of titrant, expressed in molarity.

m_{dry} is the dry mass in grams of the sample determined at 70 °C for 2 hrs under vacuum (1000 mbar).

2.3.3. Membrane argentometric titration

The quaternized membrane was dried in an oven and immersed into hydro-alcoholic (water-methanol 1:1 vol) $AgNO_3$ 0.1 N (Fluka) for 24 hrs at room temperature under magnetic stirring. Few drops of concentrated HNO_3 (Fisher) were added and the excess of Ag was titrated with HCl 0.1 N. The ion exchange capacity was calculated as follows (Eq. (3)):

$$IEC = (V_{AgNO3} - V_{HCle.p.})*[HCl]/m_{dry} \quad (3)$$

Where:

V_{AgNO3} is the initial volume, expressed in ml.

$V_{HCle.p}$ is the volume of the titrant at the equivalent point expressed in ml.

[HCl] is the concentration of titrant, expressed in molarity.

m_{dry} is the dry mass in grams of the sample determined at 70 °C for 2 hrs under vacuum (1000 mbar).

2.4. Solid-State NMR

NMR spectra were obtained on an Agilent DD2 400 MHz NB spectrometer using a 1.6 mm T3 MAS special HFXY probe at room temperature. ^{19}F, ^{1}H and $^{13}C(^{1}H)$ one pulse MAS NMR spectra were acquired a spinning speed of 28 kHz, using a 90° pulse of 3.5 μs (^{19}F), 4.0 (^{1}H and ^{13}C) and a recycle delay of 20 s (^{19}F, ^{1}H) or 25 s (^{13}C). Cross-polarization $^{13}C(^{1}H)$ CP MAS spectra were acquired at 20 kHz, using a recycle delay of 6 s and a contact time of 1 or 1.5 ms. ^{19}F chemical shifts (δ_{CS}) are reported relative to $CFCl_3$, using PTFE ($\delta_{CS} = -123$ ppm) as secondary standard. ^{1}H and ^{13}C δ_{CS} are reported relative to tetramethylsilane (TMS), using adamantane as secondary standard.

2.5. Slurry pH

The pH of slurry was measured by a glassy electrode (Metrohm Pt 1000), immersing about 0.1 g of dried polymer in 100 ml of H_2O.

2.6. Thermal analyses

Thermogravimetric analyses in terms of TGA/DSC were carried out using a thermo balance Netzsch (mod. STA 409) in air flow from room temperature up to 1000 °C with 5° min^{-1} scan rate.

Glass Transition Temperature (Tg) was determined at room humidity as Tan δ value, obtained by the ratio between elastic storage (E') and viscous loss modulus (E''). Measurements were performed as elsewhere reported [57] using a Dynamic Mechanical Analyzer Model DMA1 (Mettler Toledo, Columbus, OH, USA) on samples with Cl^- as counterions.

2.7. Water and hydroxide uptake, and dimensional swelling

The water and KOH uptakes were calculated by the difference in weight before and after the immersion of the dried alkylated membranes in water or KOH 5 wt% solution at 30 °C for 24 hrs. To reach the dry state, the samples were maintained in an oven under vacuum (1000 mbar) for 2 hrs at 70 °C.

The dimensional variation was calculated in the same operative conditions of water uptake on a rectangular sample, measuring the length (L) of the longest side.

The swelling was calculated as the ratio ΔL/L.

2.8. In-plane anion conductivity, effective mobility, diffusion coefficient

The in-plane anion conductivity of membranes, with OH^- as a counterion, was carried out in the range of temperature 30–120 °C flowing fully humidified Nitrogen, after exchanging the samples in KOH 1 M for 24 hrs at room T. The four electrodes method was used and the electrochemical impedance spectroscopy (EIS) was adopted to measure the series resistance. It was adopted a frequency range of 100 KHz – 1 Hz and a 50 mV of amplitude. The activation energy was calculated according to the Arrhenius law from the conductivity results.

The hydroxide diffusion coefficient ($cm^2\ s^{-1}$) was calculated as follows (Eq. (4):

$$D_\sigma = \sigma RT/[OH^-]F^2 \quad (4)$$

Where σ is the anion conductivity of the hydroxide form measured in humidified Nitrogen;

R is the universal gas constant (8.31 J mol^{-1} K^{-1}).

T is the temperature (K).

$[OH^-]$ is the hydroxide concentration.

F is the Faraday constant (96485C mol^{-1}).

2.9. Membrane-Electrodes assembly

For the electrodes preparation, the NiFeOx anode electrocatalyst was prepared as reported elsewhere [58]. A commercial 40 % Pt/C (HISPEC 4000 by Johnson Matthey Fuel Cell) catalyst was used at the cathode. Each catalyst slurry was prepared by mixing electrocatalysts and Fumatech FAA3 5 wt% ionomer solution as reported elsewhere [59]. The cathode ink was deposited by spray coating on carbon paper (SIGRACET 35BC) gas diffusion layers (GDL) with a total metal loading of 1 mg cm^{-2}. The anode catalyst was deposited on a Nickel felt (Bekaert) with a total catalyst loading of 2.5 mg cm^{-2}. The ionomer content in both anode and cathode catalyst layers was kept at 33 wt%. MEAs with a 5 cm^2 active area, were prepared by a cold-assembly procedure [58]. The membrane was exchanged in KOH 1 M hydro-alcoholic solution (water/ethanol 1:1 vol) for 24 hrs at room T before the assembly.

2.10. Electrochemical characterisations

The single cell was tested at different temperatures and under atmospheric pressure. KOH/water (1 M) solution was supplied by a peristaltic pump to the anode compartment, at a flow rate of 4 ml min^{-1} for all tests. Polarization curves (I-V) were performed at a scan rate of 10 mV s^{-1} with a Keithley power supply system (Tektronic). Ac-impedance analysis was used to determine the cell resistance. Series resistance (Rs) was measured from the high frequency intercept on the real axis of the Nyquist plot with a Metrohm Autolab potentiostat/galvanostat (Utrecht, The Netherlands) equipped with a Frequency Response Analyzer (FRA). The I-V curves were performed from 60 °C up to 90 °C.

3. Results and discussion

The Aquivion-SO_2F®, with 720 g mol^{-1} equivalent weight (EW), was chosen as a precursor for the quaternization reaction among the commercial products because of its hight ion exchange capacity and consequently its potentially high anion conductivity. Starting from a previous

patent [60], an optimization of the synthetic process was performed to maximize the conversion and selectivity, by selecting dispersants with very low environmental impact and low toxicity level. In detail, three different dispersants, such as Ethanol, Dimethylsufoxide and 3 M Novec 7500 were evaluated by maintaining constant the reaction time of 2 hrs and the reaction temperature of 5 °C. Various amidated products were obtained and these were characterised by different pH of slurry, as reported in Table 1. The pH of slurry of the pure solvent is reported in Table 1 as well.

The reaction was carried out in the heterophase and the use of aprotic polar solvent was necessary. As reported in Table 1 the samples AQ720A-1, AQ720A-3 and AQ720A-4 obtained using DMSO, Ethanol and Novec respectively, obtained after a reaction of 2. hrs showed a different behaviour. In fact, no amidated product was obtained for samples AQ720A-1, AQ720A-3, contrarily to sample AQ720A-4. It is expected that the introduction of an alkyl amine in the monomeric unit of the polymer, produces an increase of the pH of slurry up to about 11, typical of an alkyl amine in aqueous solution. Only the sample AQ720A-4 reached this value. Regarding AQ720A-1, prepared using DMSO, as highlighted by the slurry pH, a value approaching that found for pure DMSO (pH = 9) was obtained. A solubilization of the polymer occurs during the amidation reaction and it was supposed that the slurry pH of the final product was not realistic, but it is due to the DMSO that remained entrapped into the porosity of the polymer. To verify this hypothesis a new synthesis was carried out reducing the reaction time down to 1 h (AQ720A-2). In this case, a less solubilized polymer was obtained, and a reduced slurry pH was measured (pH = 6.6). Also, when Ethanol was used, the slurry pH of the product was slightly higher than pure ethanol, meaning that no reaction has occurred. When NOVEC 7500 was used, the slurry pH approached the value of 11 as expected for an amide. It was decided to investigate different reaction times from a minimum of 30 min to a maximum of 20 hrs. In this case, the reaction time did not affect the final product. The slurry pH was almost the same for the three synthesized products and it was considerably higher than both precursors and Novec; this means that the amidation reaction occurred with a very similar conversion factor. See Table 2..

To confirm the hypothesis of slurry pH increase when amine groups are introduced into the polymer backbone and in order to assess the structure, a solid state NMR characterization was performed. ^{19}F MAS NMR spectra were used to monitor the conversion of $–SO_2F$ moieties to $–SO_2X$ or $SO_3^-X^+$ (Fig. 1a). The signal at 44 ppm related to SO_2F can still be observed in the spectra acquired for samples AQ720A-1 and AQ720A-3, suggesting that almost no reaction occurs, whereas in the other spectra, related to Novec as solvent, this signal was no more observed. The NMR spectra demonstrate that after the reaction the polymer structure is preserved. ^1H MAS NMR spectra allowed to further investigate the obtained structure (Fig. 1b). The spectra acquired for unreacted AQ720A-1 and AQ720A-3 showed a low signal to noise ratio, suggesting that the protonated species are only residues, probably traces of DMSO and water. Samples AQ720A-4, AQ720A-5 and AQ720A-6 showed a similar spectrum. The lineshape is relatively broad and include three main contributions, at 0.8, 2.1 and 4.0 ppm. The peak at 0.8 ppm can be related to CH_3 groups in alfa position to a quaternary carbon, the peak at 2.1 ppm accounts for both CH_2 in alfa to nitrogen and CH_3 directly bonded to N. The signal at about 4 ppm is compatible with both NH groups and water molecules included in the polymer. These spectra are thus compatible with the presence of a structure $-SO_2N^{(-)}CH_2C(CH_3)_2CH_2N(CH_3)_2$.

Table 1
Synthesized amidated Aquivion-based products at 5 °C.

Sample	Solvent	Reaction time	pH_{slurry}
Aquivion-SO2F®	–	–	5.6
DMSO	–	–	9
AQ720A-1	DMSO	2 hrs	9.7
AQ720A-2	DMSO	1 h	6.6
EtOH	–	–	5.5
AQ720A-3	EtOH	2 hrs	6.2
Novec 7500	–	–	5.9
AQ720A-4	Novec	2 hrs	11.1
AQ720A-5	Novec	30 min.	11.0
AQ720A-6	Novec	20 hrs	10.7

Table 2
IEC of samples produced with different reaction times and dispersant.

Sample	Solvent	Reaction time	IEC_{NMR}, meq g^{-1}	$IEC_{t_{it-back}}$, meq g^{-1}
AQ720A-1	DMSO	2 hrs	0.08	0.05
AQ720A-3	EtOH	2 hrs	0.01	0
AQ720A-4	Novec	2 hrs	1.13	0.92
AQ720A-5	Novec	30 min.	1.13	0.80
AQ720A-6	Novec	20 hrs	1.13	0.90

The evidence that the same spectrum is observed for the samples AQ720A-4, AQ720A-5 and AQ720A-6 suggests that the reaction kinetics are very fast, and the product can be obtained already after 30 min. After a longer time, no by-products formation or secondary reactions occur, suggesting a stability of the product even after about one day (20 hrs).

It can be concluded that the synthesis carried out with Novec as dispersant converts the precursor to the desired amide product reported in Scheme 1.

Regarding the ion exchange capacity of the polymer, the measure was carried out following the back-titration procedure reported in the previous section.

It is evident that the ion exchange capacity values of the samples measured through NMR are higher than those measured through back-titration. These results are not surprising for this kind of polymer because the error in the titration method is higher than in NMR measurements [61]. The back-titration procedure, as reported in [60], is carried out in a hydro-alcoholic solution to permit the exchange of the internal anions.

The second part of the synthesis consisted in an alkylation of the tertiary amino group to form the corresponding quaternary ammonium salt. The synthesis was carried out starting from sample AQ720A-5 and obtaining the sample AQ720A-5-Q1.

The ^1H MAS NMR spectrum acquired for this sample is reported in Fig. 1b. We can observe additional contributions to the spectrum, in particular, the relatively sharp signal at 3.1 ppm, which is compatible with the structure $(CH_3)_3N^+$, and the double peak centered at 7.2 ppm, which includes the peak at 7.6 ppm due to aromatic protons and the peak at 6.9 ppm, which could be related to both residual unreacted SO_3H of methyl tosylate and water coordinated with both SO_3H and SO_3^-. ^{13}C MAS NMR spectra can be also useful for investigating the product obtained after quaternization (AQ720A-5-Q1). The spectra of sample AQ720A-5 and AQ720A-5-Q1 are compared in Fig. 2.

In the spectrum acquired for AQ720A-5, four main signals can be observed at 111, 47, 36, and 24 ppm. The very large signal at 111 ppm is related to the fluorinated polymer. The signal has a low intensity because the CF_2 groups receive only a small fraction of magnetization from protons in a $^1H \rightarrow ^{13}C$ CP experiment and is also poorly resolved due to the absence of fluorine-decoupling. The peak at 24 ppm can be attributed to CH_3 in α- position to a quaternary carbon, and the signal at 47 ppm can be attributed to CH_3 directly bonded to nitrogen. The signal at 36 ppm can be attributed to CH_2. The very small and sharp contribution at 17 ppm could be attributed to residual ethanol trapped in the polymer during the washing step. The spectrum of the sample after quaternization (AQ720-A-5-Q1) shows additional signals and a shift of some of the signals already present in the previous synthetic step. The signals from 144 to 127 ppm are related to the carbon atoms of the aromatic ring, whereas the CH_3 linked to the aromatic ring resonates at 20 ppm. Hence, the presence of a derivative of *p*-toluenesulfonic acid can be confirmed. The peak at 144 ppm accounts for the quaternary carbon in alpha to CH_3, whereas the quaternary carbon in alpha to the sulfonic

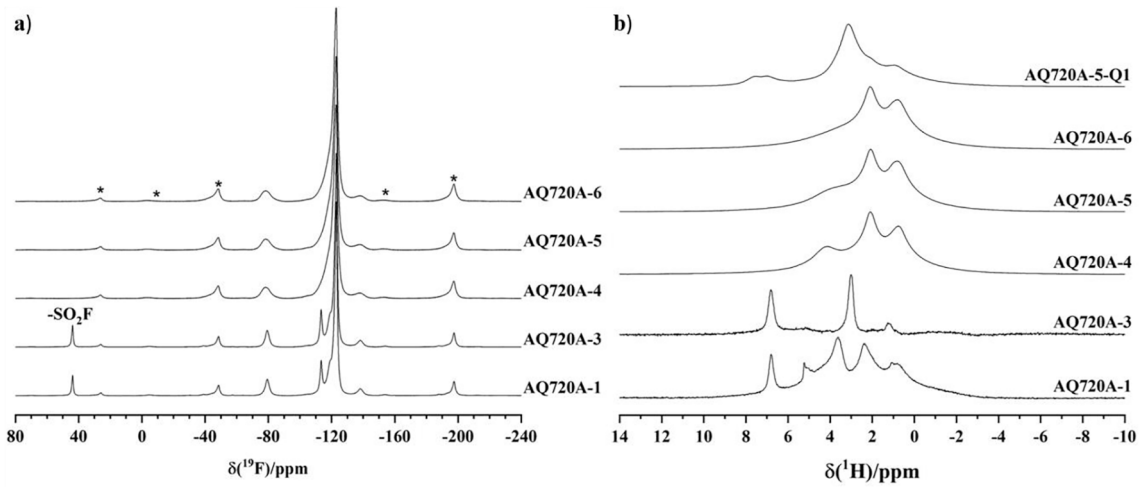

Fig. 1. Solid-State NMR characterization: a)^{19}F MAS spectra for samples AQ720A-1 to AQ720A-6, peaks marked with an asterisk are spinning sidebands of the main signals; b) ^{1}H MAS spectra for samples AQ720A-1 to AQ720A-6 and 1 AQ720A-5-Q1.

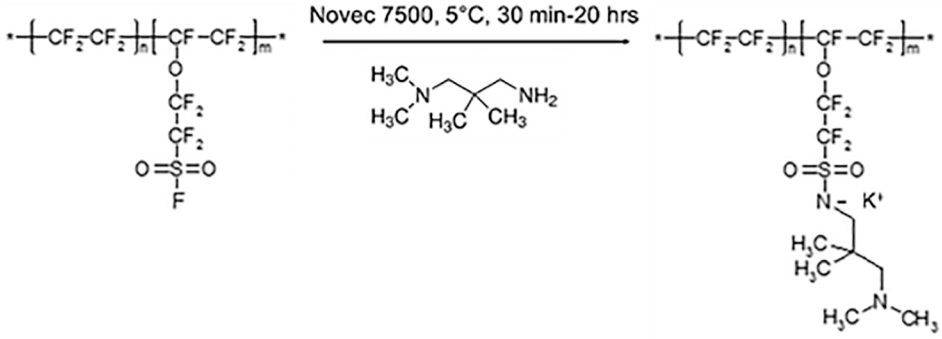

Scheme 1. Amidation reaction.

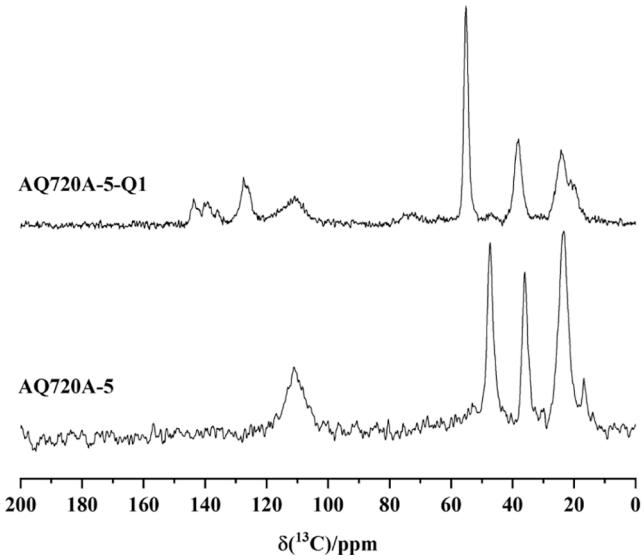

Fig. 2. ^{13}C(^{1}H) CP MAS spectra of AQ720A-5 and AQ720A-5-Q1 recorded with 1 ms as contact time.

moieties exhibits two resonances at 139 and 136 ppm, further corroborating the hypothesis of the presence of both a neutral and a salt form. The other carbons of the aromatic ring resonate at 128 ppm. The remaining contributions to the spectrum, which were already observed in AQ720A-5, show some changes due to the presence of the p-toluene sulfonic acid derivative. The signal at 36 ppm is now shifted at 38 ppm, suggesting a change in the chemical environment explored by CH_2 groups. The signal at 47 ppm now has a very low intensity, but there is a new resonance at 55 ppm compatible with the structure $(CH_3)_3$-$N^{+\cdot}$ This evidence suggests that most of the CH_3 groups in alpha to nitrogen belong to the salt form., i.e. that the quaternary reaction successfully occurs. The small featureless contribution centred at about 72 ppm could be tentatively assigned to quaternary carbons. Such contribution could now be observed due to an improved efficiency of the CP experiment, also suggested by the overall better resolution of the recoded spectrum. The steric hindrance induced by the presence of the aromatic derivate, slows down the chain motions of the alkyl chains resulting in an improved efficiency of the ^{1}H →^{13}C magnetization transfer.

According to these results it can be concluded that a quaternarization reaction occurred and the quaternary ammonium-based polymer product was obtained following the Scheme 2.

In Table 3 the pH_{slurry} and IEC variations as a function of the synthesis steps are reported.

The pH_{slurry} value, that gives information about the acidity or alkalinity of the sample, increases after the amidation reaction and it is reduced after the alkylation step, meaning that the salt formation occurred, as reported in Scheme 2. In addition, it was demonstrated from NMR data that the complete conversion from amidated product in alkylated occurs. A change of the IEC from 1.13 meq g^{-1} (amidated product) to 1.10 meq g^{-1}corresponding to the quaternary ammonium formation, as reported in scheme 2 was observed.

To understand the thermal stability of the polymer after each reaction step, thermogravimetric analyses were carried out from room

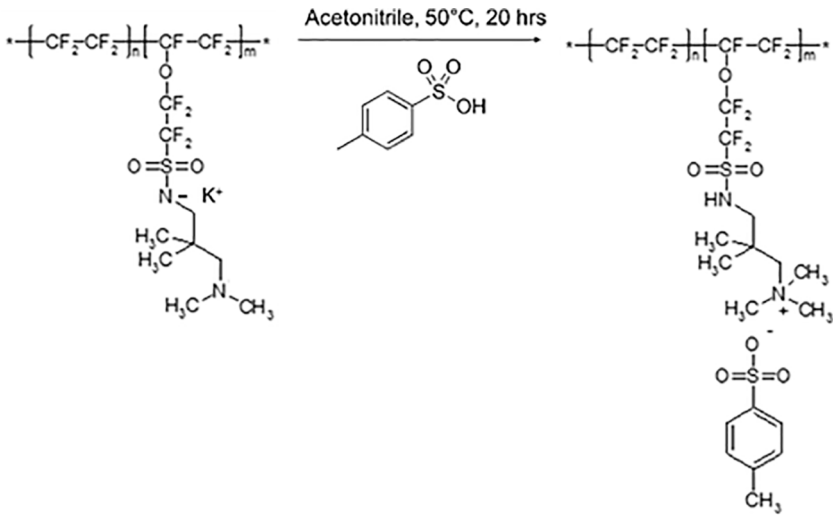

Scheme 2. Alkylation reaction.

Table 3
Comparison of the physico-chemical characteristics.

Sample	Yield, %	pH_{slurry}	IEC $_{NMR}$, meq g^{-1}
AQ720-SO2F	–	5.6	1.39
AQ720A-5	76	11.0	1.13
AQ720A-5-Q1	78	6.5	1.10

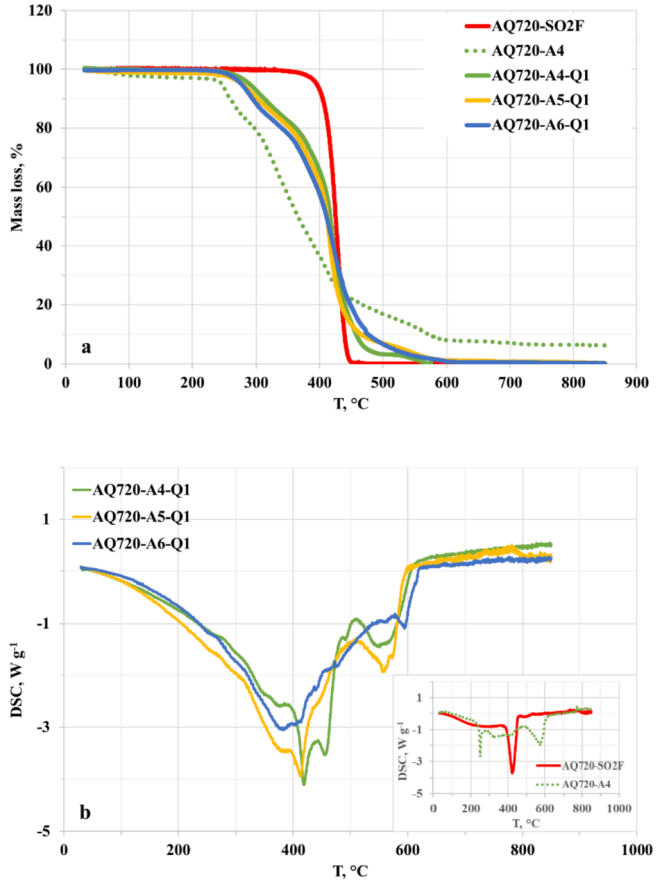

Fig. 3. Thermal profiles of the synthesized polymers compared to the precursor. a) thermogravimetry, b) differential scanning calorimetry.

temperature up to 1000 °C in air flow with 5 °C min^{-1} scan rate.

In Fig. 3, a comparison of the thermal profiles (thermogravimetry and differential scanning calorimetry) for the precursor, the amidated product and the quaternized ones are reported.

The thermal profile of polymer with SO_2F groups shows a degradation starting at about 400 °C, related to the decomposition of the fluorosulfonyl group and the main chain of the polymer. Regarding the amidated products, the sample AQ720A-4 is reported as example because the other show the same behaviour. The introduction of functional groups modifies the thermal profile with respect to the precursor. The first mass loss from room T to about 150 °C is attributable to the water loss (3.8 % and 1.2 % for AQ720A-4 and AQ720A-4-Q1, respectively), the second loss in the range 230–350 °C is due to the functional groups decomposition and the third one, over 350 °C, is attributable to the decomposition process of the polymer main chain (Fig. 3).

As reported for the $–SO_3H$ form, the conversion of the sulfonyl fluoride group decreases the decomposition temperature from about 400 °C down to about 250 °C (AQ720A-4). In any case, at lower temperatures, no mass losses except the water loss, are detectable, meaning a good thermal stability towards the oxidation process at high temperature. The curve of the AQ720A-4 sample presents a residual mass over the decomposition temperature of the polymer backbone; this mass can be attributed to the formation of a potassium salt K_2SO_4, formed during the decomposition process. In particular, the melting temperature of potassium sulphate occurs at 1069 °C and this can explain the residual mass observed. This hypothesis is supported by the literature, in fact a similar behaviour was found for a polyaromatic in sodium salt form and for perfluorosulphonic salt membrane [62,63]. The alkylation synthesis increases the decomposition temperature of the functional group of about 20 °C, due to the quaternary ammonium salt formation having tosylate as a counter-anion. In addition, the absence of a residual mass at high temperature indicates that no residual K^+ is present and this means a complete conversion of the polymer to the quaternary form. Moreover, the mass loss obtained up to 150 °C suggests that no free unreacted species should be present in the sample, otherwise a value higher than 1.2 % should be observed, due to the hydrophilic properties of methyl tosylate.

From DSC curves, an endothermic peak at 150 °C is visible for sample AQ720A-4 which is associated to the side chains degradation, as also reported in ref. [55]. This peak is no more detectable after the alkylation reaction (samples AQ720A-4-Q1, AQ720A-5-Q1 and AQ720A-6-Q1). Only a broad peak is visible related to the degradation of the backbone and the side polymer chains.

The thermal profile of the quaternized products is quite similar,

meaning a successful reaction. The sample AQ720A-4-Q1 seems to have a slightly higher thermal stability than other samples, also confirmed from the slight shift of DSC peak at higher temperatures. This result makes the polymer a good candidate for the application in AEM water electrolysis working at temperatures higher than conventional systems (60 °C).

The sample obtained after 2 hrs of amidation reaction (AQ720A-4-Q1) was chosen for the further investigations, resulting from the best compromise among reduced reaction time, thermal stability and complete conversion in quaternized product.

A membrane (AQ720A-4-Q) was prepared, following the procedure described in section 2.2, and characterised in terms of physico-chemical parameters. In Table 4 the IEC of fluorinated AEM in the presence of chloride and hydroxide counter-ions is reported. The sample in Cl^- form was exchanged for 24 hrs in KOH 1 M at room temperature and then the IEC_{OH} was determined by acid-base back-titration. The data were compared to the commercial membrane FAA3-50, considered in this work as a reference, to understand the stability of the functional groups in alkaline environment.

According to the data reported in Table 4, the sample AQ720A-4-Q presents an IEC loss of 2 % passing from Cl^- form to OH^-, meaning a good stability when immersed in high pH level solution. On the contrary the FAA3-50 membrane showed a large loss (about 14 %) after immersion in alkaline environment.

To further confirm the stability of Aquivion® based membranes at high temperatures, water uptake, swelling and other physico-chemical data were measured at 90 °C (Table 5). No comparison was possible with the reference membrane at high temperature due to the excessive swelling of the FAA3-50; thus, the data obtained at room temperature were used.

According to Table 5, it is evident that the Aquivion® AEM shows a larger number of water molecules coordinated to the quaternary ammonium group (λ) than the FAA3-50, due to similar water uptake and lower IEC values. The swelling measured as length variation (ΔL/L %) is the same while the area variation (A %) is higher for the AQ720A-4-Q membrane. Regarding the swelling calculated as volume variation, this is lower than the critical value of 2 for the Aquivion® membrane while this is more than twice for FAA3-50. Although the hydroxide concentration is, obviously, lower for the AQ720A-4-Q sample, the higher water content in the conductive hydrophilic clusters, leads to a better ion mobility. In general, ion mobility (μ_{eff}) provides information about the acidic/alkaline dissociation degree, ionic channel tortuosity and spatial proximity of neighbouring acidic/alkaline groups. The value 1.99 10^{-4} cm^2 V^{-1} s^{-1} observed for Aquivion® membrane, one order of magnitude higher than that of FAA3-50, is associated to a good dissociation of anions due to the presence of fluorine atoms in the side chains. These results are in accordance to that reported in the literature for similar polymer membranes [64].

The glass transition was found to be higher for FAA3-50 membrane than Aquivion®. The Fig. representing the tan delta curve is reported in SI1. This result is in accordance to what reported previously for proton exchange membrane based on the same polymer perfluorinated backbone whereas the FAA3 membrane is based on a polysulfone (PSF) backbone [65]. In a previous paper, it was reported that the glass transition of the bare PSF at 190 °C increased over 200 °C when the sulphonic functional group was inserted in the main chain [63]. The result found for the FAA3-50 is in accordance with the literature, because the introduction of quaternary ammonium groups in the PSF aromatic rings supplies a more rigid structure increasing the T_g. Regarding the Aquivion® membrane, a glass transition of about 150 °C for sulphonated polymer was found [66–68] for polymers with a 720–790 g mol^{-1} EW. This value increases to about 195 °C (tab.5) when quaternary ammonium groups are inserted instead of sulphonic groups, producing a more rigid structure due to the high steric hindrance due to the dimensions of the functional groups.

Table 4
Samples AQ720A-4-Q1 Ion exchange capacity.

Membrane	Anion	IEC_{Cl}, meq g^{-1}	Anion	IEC_{OH}, meq g^{-1}	*IEC loss, %
FAA3-50	Cl	1.85	OH	1.59	14
AQ720A-4-Q	Cl	0.86	OH	0.84	2

* after immersing 1 M KOH solution for 24 hrs.

The membrane AQ720A-4-Q was also characterized in terms of conductivity measurements and compared to the commercial reference. In Fig. 4, it is reported the hydroxide diffusion coefficient as a function of the temperature, as calculated in section 2.9. It is evident that the diffusion coefficient for the two membranes is very similar at low temperature and a more pronounced difference is found at high temperature. This behaviour could be attributable to the high swelling level of FAA3 at T > 60 °C that produces higher water uptake and lower hydroxide concentration values with an improved ion mobility.

In any case, the values found for both membranes are in the order of magnitude of 10^{-6} cm^2 s^{-1} and comparable to what reported in literature for similar membranes [69,59].

Since the OH^- diffusion coefficient, shows an Arrhenius behaviour, in the temperature range 30–90 °C, the activation energy can be calculated accordingly. It corresponds to 27.4 kJ mol^{-1} for the commercial membrane and 26.1 kJ mol^{-1} for Aquivion®-based membrane. The activation energy is very similar for both samples and these values suggest that the anion conductivity is mainly ruled by the Grotthuss mechanism instead of the vehicular one [70].

The polarization curves in an electrolysis single cell, operating at 60 °C, are reported for both the Aquivion® membrane and the benchmark membrane (FAA3-50) in Fig. 5.

Even if the performance is lower than the benchmark membrane, to our best knowledge, the data here achieved for the Aquivion®-based anion exchange membranes favourably compare to those reported in the literature for fluorinated anion-exchange membranes [51,53,71–74]. To further verify the performance at temperatures higher than 60 °C, where the benchmark membrane degrades drastically due to a high swelling with a drop of mechanical properties, the polarization curves for the Aquivion®-based membrane are shown up to 90 °C in Fig. 6.

The performance increases with the temperature, meaning that the optimal operating temperature for this fluorinated polymer is higher than those conventional used for AEM based systems (50–60 °C). A current density of 0.9 A cm^{-2} at 2.2 V was achieved at 90 °C with a voltage efficiency of 70 %. The latter is determined from the ratio between the thermoneutral voltage and the operating cell potential. In addition, the series resistance determined from EIS measurements (Table 6), highlights the benefit of the increase of temperature. In fact, a reduction of about 50 % of the series resistance (Rs) can be observed when the temperature is increased from 60 °C to 90 °C. Moreover, a voltage efficiency (V_{eff}) of 80 % at 0.5 A cm^{-2} (a typical operating current density in alkaline electrolysis) is achieved showing promising characteristics of this polymer membrane for application in electrochemical water splitting processes.

The preliminary results, reported in this study for an Aquivion®-based anion exchange membrane, clearly evidence the promising characteristics of this novel membrane for application in AEMWE electrochemical devices, in particular at temperatures higher the conventional 50–60 °C used in anion exchange membrane water electrolysis. This has relevant implications in terms of enhanced reaction kinetics and minimization of catalyst loadings.

4. Conclusions

A simple two-steps procedure for the production of an anion exchange Aquivion®-based membrane was developed. Reaction parameters, such as polymer dispersant and reaction time were optimised.

Table 5
Physico chemical data @ 90 °C for Aquivion® membrane compared to FAA3-50 @ 30 °C.

Membrane	λ	w.u., %	ΔL/L, %	A, %	Vwet/Vdry	[OH], M	μ_{eff}, $cm^2\ V^{-1}s^{-1}$	T_g, °C
FAA3-50	6	17	9	7	5	1.5	6.27 10–5	210
AQ720A-4-Q	20.3	21.9	9	21.0	1.2	0.88	1.99 10–4	195

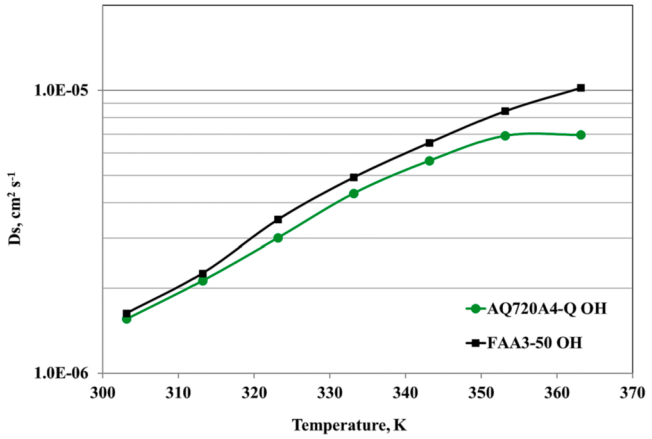

Fig. 4. Diffusion coefficient versus temperature.

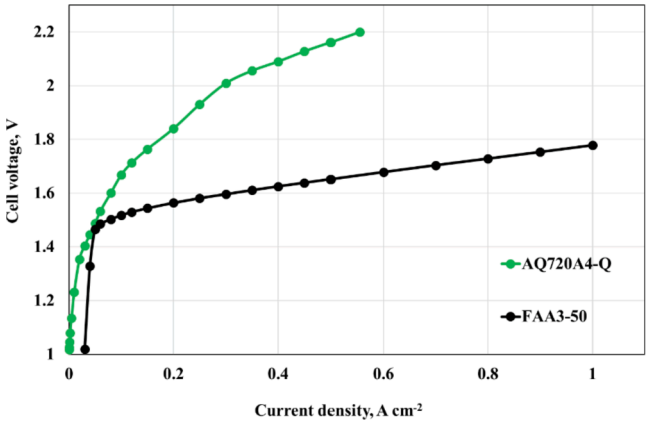

Fig. 5. Comparison of water electrolysis I-V curves for FAA3-50 and AQ720A-4-Q membranes at 60 °C.

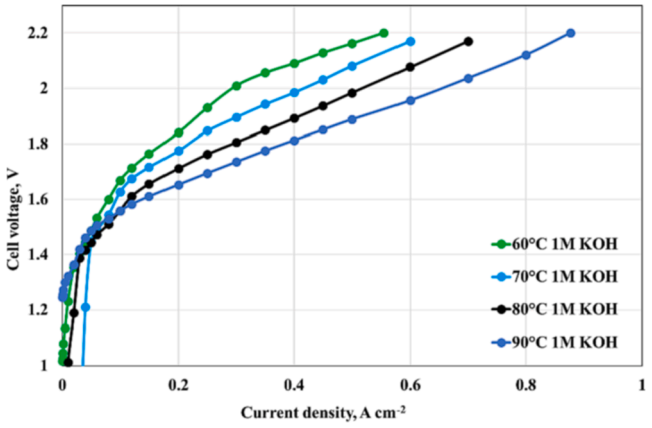

Fig. 6. Water electrolysis polarization curves at different temperatures carried out with the AQ720A4-Q membrane.

Table 6
Electrochemical data at different temperatures.

T_{cell}, °C	Rs, Ωcm^2	V eff @ 0.5 A cm^{-2}, %
60	0.91	68
70	0.82	71
80	0.56	76
90	0.49	79

Novec was selected as the best dispersant while a reaction of 2 hrs at 5 °C was chosen as the best approach for the alkylation reaction. A simple method for the conversion of alkyl groups into a quaternay ammonium salt was also developed. An in-depth solid state NMR study demonstrated the quantitative conversion of the groups as a function of the reaction parameters. A good thermal stability was observed for the membrane with a glass transition temperature approaching 200 °C. Limited swelling was observed at 90 °C, i.e. at an operating temperature higher than the conventional one (T ~ 50 °C) presently used for anion exchange membrane water electrolysis. This means a potential extension of the operating temperature for this technology with an associated enhancement of reaction kinetics. A diffusion coefficient in the order of magnitude of 10^{-6} $cm^2\ s^{-1}$ was measured, comparable to what reported in literature for similar AEM. The activation energy suggests an anion conductivity mainly governed by the Grotthuss mechanism. Water electrolysis polarization curves have shown a current density of 0.9 A cm^{-2} at 2.2 V at 90 °C with voltage efficiency approaching 70 %. A voltage efficiency (V_{eff}) of about 80 % was recorded at 0.5 A cm^{-2}, a typical operating current density in alkaline electrolysis. The promising physico-chemical and electrochemical properties observed for the Aquivion® AEM operating at 90 °C clearly indicate the possibility of extending the operating temperature range with relevant implications in terms of better thermal management at high current density, enhanced reaction rate and possibility to minimize expensive electrocatalysts.

Declaration of Competing Interest

The authors declare that they have no known competing financial interests or personal relationships that could have appeared to influence the work reported in this paper.

Data availability

Data will be made available on request.

Acknowledgements

"The authors acknowledge the financial support provided by the ANIONE project under the European Union's Horizon 2020 Research and Innovation Programme. This project has received funding from the Fuel Cells and Hydrogen 2 Joint Undertaking (now Clean Hydrogen Partnership) under Grant Agreement No 875024. This Joint Undertaking receives support from the European Union's Horizon 2020 Research and Innovation program, Hydrogen Europe and Hydrogen Europe Research and Italy, France, United Kingdom, Denmark, Belgium, Netherlands, Israel. The authors are also grateful to NV BEKAERT SA (Belgium) for the supply of Ni backing layers."

References

[1] https://ec.europa.eu/clima/eu-action/climate-strategies-targets/2030-climate-energy-ramework_en.

[2] E. Marzi, M. Morini, A. Gambarotta, Analysis of the status of research and innovation actions on electrofuels under horizon 2020, Energies 15 (2022) 618, https://doi.org/10.3390/en15020618.

[3] D. Li, A.R. Motz, C. Bae, C. Fujimoto, G. Yang, F.-Y. Zhang, K.E. Ayers, Y. Seung Kim, Durability of anion exchange membrane water electrolyzers, Energy Environ. Sci. 14 (2021) 3393, https://doi.org/10.1039/d0ee04086j.

[4] Y. Seung Kim, Polymer electrolytes with high ionic concentration for fuel cells and electrolyzers, ACS Appl. Polym. Mater. 3 (2021) 1250–1270, https://doi.org/10.1021/acsapm.0c01405.

[5] B.J.M. Etzold, U. Krewer, S. Thiele, A. Dreizler, E. Klemm, T. Turek, Understanding the activity transport nexus in water and CO2 electrolysis: State of the art, challenges and perspectives, Chem. Eng. J. 424 (2021), 130501, https://doi.org/10.1016/j.cej.2021.130501.

[6] J.-C. Kim, J. Kim, J.C. Park, S.H. Ahn, D.-W. Kim, Ru2P nanofibers for high-performance anion exchange membrane water electrolyzer, Chem. Eng. J. 420 (2021), 130491, https://doi.org/10.1016/j.cej.2021.130491.

[7] L. Wan, Z. Xu, B. Wang, Green preparation of highly alkali-resistant PTFE composite membranes for advanced alkaline water electrolysis, Chem. Eng. J. 426 (2021), 131340, https://doi.org/10.1016/j.cej.2021.131340.

[8] M. Zeppilli, A. Lai, M. Villano, M. Majone, Anion vs cation exchange membrane strongly affect mechanisms and yield of CO2 fixation in a microbial electrolysis cell, Chem. Eng. J. 304 (2016) 10–19, https://doi.org/10.1016/j.cej.2016.06.020.

[9] C. López-Fernández, J. Gómez-Sacedón, J.P. Gil-Rostra, A.R. Espinós, F. González-Elipe, F. Yubero, A. de Lucas-Consuegra, Ionomer-free nickel-iron bimetallic electrodes for efficient anion exchange membrane water electrolysis, Chem. Eng. J. 433 (2022), 133774, https://doi.org/10.1016/j.cej.2021.133774.

[10] A.Y. Faid, A.O. Barnett, F. Seland, S. Sunde, Tuning Ni−MoO2 catalyst−ionomer and electrolyte interaction for water electrolyzers with anion exchange membranes, ACS Appl. Energy Mater. 4 (2021) 3327–3340, https://doi.org/10.1021/acsaem.0c03072.

[11] E. Cossar, A.O. Barnett, F. Seland, E.A. Baranova, The performance of nickel and nickel-iron catalysts evaluated as anodes in anion exchange membrane water electrolysis, Catalysts 9 (2019) 814, https://doi.org/10.3390/catal9100814.

[12] A.Y. Faid, L. Xie, A.O. Barnett, F. Seland, D. Kirk, S. Sunde, Effect of anion exchange ionomer content on electrode performance in AEM water electrolysis, Int. J. Hydrogen Energy 45 (2020) 28272–28284, https://doi.org/10.1016/j.ijhydene.2020.07.202.

[13] V.M. Truong, J.R. Tolchard, J. Svendby, M. Manikandan, H.A. Miller, S. Sunde, H. Yang, D.R. Dekel, A.O. Barnett, Platinum and platinum group metal-free catalysts for anion exchange membrane fuel cells, Energies 13 (2020) 582, https://doi.org/10.3390/en13030582.

[14] E. Cossar, A.O. Barnett, F. Seland, R. Safari, G.A. Botton, E.A. Baranova, Ionomer content optimization in nickel-iron-based anodes with and without ceria for anion exchange membrane water electrolysis, J. Power Sources 514 (2021), 230563, https://doi.org/10.1016/j.jpowsour.2021.230563.

[15] P. Fortin, T. Khoza, X. Cao, S.Y. Martinsen, A.O. Barnett, S. Holdcroft, High-performance alkaline water electrolysis using Aemion™ anion exchange membranes, J. Power Sources 451 (2020), 227814, https://doi.org/10.1016/j.jpowsour.2020.227814.

[16] A.Y. Faid, A.O. Barnett, F. Seland, S. Sunde, NiCu mixed metal oxide catalyst for alkaline hydrogen evolution in anion exchange membrane water electrolysis, Electrochim. Acta 371 (2021), 137837, https://doi.org/10.1016/j.electacta.2021.137837.

[17] A.Y. Faid, A.O. Barnett, F. Seland, S. Sunde, Ternary NiCoFe nanosheets for oxygen evolution in anion exchange membrane water electrolysis, Int. J. Hydrogen Energy 47 (2022) 23483–23497, https://doi.org/10.1016/j.ijhydene.2022.05.143.

[18] L. Wang, T. Weissbach, R. Reissner, A. Ansar, A.S. Gago, S. Holdcroft, K. Andreas Friedrich, High performance anion exchange membrane electrolysis using plasma-sprayed, non-precious-metal electrodes, ACS Appl. Energy Mater. 2 (2019) 7903–7912, https://doi.org/10.1021/acsaem.9b01392.

[19] A. S. Ansar, A. S. Gago, F. Razmjooei, R. Reißner, Z. Xu, K. A. Friedrich, Alkaline electrolysis—status and Prospects, in J. Garche and K. Brandt (Eds.), Electrochemical Power Sources: Fundamentals, Systems, and Applications. Elsevier, 2018 pp. 165-198 https://doi.org/10.1016/B978-0-12-819424-9.00004-5.

[20] F. Razmjooei, A. Farooqui, R. Reissner, A.S. Gago, S.A. Ansar, K.A. Friedrich, Elucidating the performance limitations of alkaline electrolyte membrane electrolysis: dominance of anion concentration in membrane electrode assembly, ChemElectroChem 7 (2020) 3951–3960, https://doi.org/10.1002/celc.202000605.

[21] L. Wang, V.A. Saveleva, M.J. Eslamibidgoli, D. Antipin, C. Bouillet, I. Biswas, A. S. Gago, S.S. Hosseiny, P. Gazdzicki, M.H. Eikerling, E.R. Savinova, K.A. Friedrich, Deciphering the exceptional performance of NiFe hydroxide for the oxygen evolution reaction in an anion exchange membrane electrolyzer, ACS Appl. Energy Mater. 5 (2022) 2221–2230, https://doi.org/10.1021/acsaem.1c03761.

[22] F. Razmjooei, T. Morawietz, E. Taghizadeh, E. Hadjixenophontos, L. Mues, M. Gerle, B.D. Wood, C. Harms, A.S. Gago, S. Asif Ansar, K.A. Friedrich, Increasing the performance of an anion-exchange membrane electrolyzer operating in pure water with a nickel-based microporous layer, Joule 5 (2021) 1776–1799, https://doi.org/10.1016/j.joule.2021.05.006.

[23] F. Razmjooei, R. Reißner, A.S. Gago, A. Ansar, Highly active binder free Plasma sprayed non-noble metal electrodes for anion exchange membrane electrolysis at different reduced KOH concentrations, ECS Trans. 92 (2019) 689–702, https://doi.org/10.1149/09208.0689ecst.

[24] C. Santoro, A. Lavacchi, P. Mustarelli, V. Di Noto, L. Elbaz, D.R. Dekel, F. Jaouen, What is next in anion-exchange membrane water electrolyzers? bottlenecks, benefits, and future, ChemSusChem 15 (2022) e202200027.

[25] N. Du, C. Roy, R. Peach, M. Turnbull, S. Thiele, C. Bock, Anion-exchange membrane water electrolyzers, Chem. Rev. 122 (2022) 11830–11895, https://doi.org/10.1021/acs.chemrev.1c00854.

[26] G. Das, J.-H. Choi, P.K.T. Nguyen, D.-J. Kim, Y.S. Yoon, Anion exchange membranes for fuel cell application: a review, Polymers 14 (2022) 1197, https://doi.org/10.3390/polym14061197.

[27] J.S. Olsson, T.H. Pham, P. Jannasch, Poly(arylene piperidinium) hydroxide ion exchange membranes: synthesis, alkaline stability, and conductivity, Adv. Funct. Mater. (2017) 1702758, https://doi.org/10.1002/adfm.201702758.

[28] V.D.C. Tinh, V.D. Thuc, Y. Jeon, G.-Y. Gu, D. Kim, Highly durable poly(arylene piperidinium) composite membranes modified with polyhedral oligomeric silsesquioxane for fuel cell and water electrolysis application, J. Memb. Sci. 660 (2022), 120903, https://doi.org/10.1016/j.memsci.2022.120903.

[29] K.M. Meek, C.M. Antunes, D.J. Strasser, Z.R. Owczarczyk, A.C. Yang-Neyerlin, B. S. Pivovar, High-throughput anion exchange membrane characterization at NREL, ECS Transactions 92 (8) (2019) 723–731, https://doi.org/10.1149/09208.0723ecst.

[30] T.H. Pham, J.S. Olsson, P. Jannasch, Poly(arylene alkylene)s with pendant N-spirocyclic quaternary ammonium cations for anion exchange membranes, J. Mater. Chem. A 6 (2018) 16537, https://doi.org/10.1039/c8ta04699a+.

[31] E. López-Fernández, C. Gómez Sacedón, J. Gil-Rostra, F. Yubero, A.R. González-Elipe, A. de Lucas-Consuegra, Recent advances in alkaline exchange membrane water electrolysis and electrode manufacturing, Molecules 26 (2021) 6326, https://doi.org/10.3390/molecules26216326.

[32] K.H. Gopi, S.D. Bhat, Anion exchange membrane from polyvinyl alcohol functionalized with quaternary ammonium groups via alkyl spacers, Ionics 24 (2018) 1097–1109, https://doi.org/10.1007/s11581-017-2272-x.

[33] Z. Xu, L. Wan, Y. Liao, K. Peican Wang, B.W. Liu, Anisotropic anion exchange membranes with extremely high water uptake for water electrolysis and fuel cells, J. Mater. Chem. A 9 (2021) 23485–23496, https://doi.org/10.1039/d1ta06579c.

[34] A. Carbone, R. Pedicini, I. Gatto, A. Saccà, A. Patti, G. Bella, M. Cordaro, Development of polymeric membranes based on quaternized polysulfones for AMFC applications, Polymers 12 (2020) 283, https://doi.org/10.3390/polym12020283.

[35] I. Vincent, D. Bessarabov, Low cost hydrogen production by anion exchange membrane electrolysis: a review, Renewable Sustainable Energy Rev. 81 (2018) 1690–1704, https://doi.org/10.1016/j.rser.2017.05.258.

[36] A. Konovalova, H. Kim, S. Kim, A. Lim, H.S. Park, M.R. Kraglund, D. Aili, J.H. Jang, H.-J. Kim, D. Henkensmeier, Blend membranes of polybenzimidazole and an anion exchange ionomer (FAA3) for alkaline water electrolysis: Improved alkaline stability and conductivity, J. Memb. Sci. 564 (2018) 653–662, https://doi.org/10.1016/j.memsci.2018.07.074.

[37] D. Henkensmeier, M. Najibah, C. Harms, J. Žitka, J. Hnát, K. Bouzek, Overview: state-of-the art commercial membranes for anion exchange membrane water electrolysis, J. Electrochem. Energy Convers. Storage 18 (2021) 02400–02401, https://doi.org/10.1115/1.4047963.

[38] B. Chen, P. Mardle, S. Holdcroft, Probing the effect of ionomer swelling on the stability of anion exchange membrane water electrolyzers, J. Power Sources 550 (2022), 232134, https://doi.org/10.1016/j.jpowsour.2022.232134.

[39] J. Xue, J. Zhang, X. Liu, T. Huang, H. Jiang, Y. Yin, Y. Qin, M.D. Guiver, Toward alkaline-stable anion exchange membranes in fuel cells: cycloaliphatic quaternary ammonium-based anion conductors, Electrochem. Energy Rev 5 (2022) 348–400, https://doi.org/10.1007/s41918-021-00105-7.

[40] J.R. Varcoe, P. Atanassov, D.R. Dekel, A.M. Herring, M.A. Hickner, P.A. Kohl, A. R. Kucernak, W.E. Mustain, K. Nijmeijer, K. Scott, T. Xuk, L. Zhuangl, Anion-exchange membranes in electrochemical energy systems, Energy Environ. Sci. 7 (2014) 3135–3191, https://doi.org/10.1039/C4EE01303D.

[41] M.l R. Kraglund, D. Aili, K. Jankova, E. Christensen, Q. Li, J.O. Jensen, Zero-gap alkaline water electrolysis using ion-solvating polymer electrolyte membranes at reduced KOH concentrations, J. Electrochem. Soc. 163 (2016) F3125, https://doi.org/10.1149/2.0161611jes.

[42] D. Aili, M.K. Hansen, J.W. Andreasen, J. Zhang, J.O. Jensen, N.J. Bjerrum, Q. Li, Porous poly(perfluorosulfonic acid) membranes for alkaline water electrolysis, J. Memb. Sci. 493 (2015) 589–598, https://doi.org/10.1016/j.memsci.2015.06.057.

[43] K.H. Gopi, V.M. Dhavale, S.D. Bhat, Development of polyvinyl alcohol/chitosan blend anion exchange membrane with mono and di quaternizing agents for application in alkaline polymer electrolyte fuel cells, Mater. Sci. Energy Technol. 2 (2019) 194–202, https://doi.org/10.1016/j.mset.2019.01.010.

[44] W. Jiang, A.Y. Faid, B. Ferreira Gomes, I. Galkina, L. Xia, C.M. Silva Lobo, M. Desmau, P. Borowski, H. Hartmann, A. Maljusch, A. Besmehn, C. Roth, S. Sunde, W. Lehnert, M. Shviro, Composition-dependent morphology, structure, and catalytical performance of nickel-iron layered double hydroxide as highly-efficient and stable anode catalyst in anion exchange membrane water electrolysis, Adv. Funct. Mater. 32 (2022) 2203520, https://doi.org/10.1002/adfm.202203520.

[45] B. Endrodi, E. Kecsenovity, A. Samu, T. Halmagyi, S. Rojas-Carbonell, L. Wang, Y. Yan, C. Janaky, High carbonate ion conductance of a robust PiperION membrane allows industrial current density and conversion in a zero-gap carbon dioxide electrolyzer cell, Energy Environ. Sci. 13 (2020) 4098, https://doi.org/10.1039/d0ee02589e.

[46] R.A. Krivina, G.A. Lindquist, M.Y. Chieh, A.K. Cook, C.H. Hendon, A.R. Motz, C. Capuano, K.E. Ayers, J.E. Hutchison, S.W. Boettcher, Three-electrode study of electrochemical ionomer degradation relevant to anion-exchange-membrane water electrolyzers, ACS Appl. Mater. Interfaces 14 (2022) 18261–18274, https://doi.org/10.1021/acsami.1c22472.
[47] J. Xiao, A.M. Oliveira, L. Wang, Y. Zhao, T. Wang, J. Wang, B.P. Setzler, Y. Yan, Water-fed hydroxide exchange membrane electrolyzer enabled by a fluoride-incorporated nickel−iron oxyhydroxide oxygen evolution electrode, ACS Catal. 11 (2021) 264–270, https://doi.org/10.1021/acscatal.0c04200.
[48] H. Khalid, M. Najibah, H.S. Park, C. Bae, D. Henkensmeier, Properties of anion exchange membranes with a focus on water electrolysis, Membranes 12 (2022) 989, https://doi.org/10.3390/membranes12100989.
[49] L. Shi, Y. Zhao, S. Matz, S. Gottesfeld, B.P. Setzler, Y. Yan, A shorted membrane electrochemical cell powered by hydrogen to remove CO2 from the air feed of hydroxide exchange membrane fuel cells, Nature Energy (2022), https://doi.org/10.1038/s41560-021-00969-5.
[50] G.A. Lindquist, S.Z. Oener, R. Krivina, A.R. Motz, A. Keane, C. Capuano, K.E. Ayers, S.W. Boettcher, Performance and durability of pure-water-fed anion exchange membrane electrolyzers using baseline materials and operation, ACS Appl. Mater. Interfaces 13 (2021) 51917–51924, https://doi.org/10.1021/acsami.1c06053.
[51] S.A. Lee, J. Kim, K.C. Kwon, S.H. Park, H.W. Jang, Anion exchange membrane water electrolysis for sustainable large-scale hydrogen production, Carbon Neutralization 1 (2022) 26–48, https://doi.org/10.1002/cnl2.9.
[52] P. Stilli, S. Bonizzoni, F. Lohmann-Richters, L. Beverina, A. Papagni, P. Mustarelli, Electrochim. Acta 405 (2022), 139834, https://doi.org/10.1016/j.electacta.2022.139834.
[53] S. Lee, H. Lee, T.-H. Yang, B. Bae, N.A. Thu Tran, Y. Cho, N. Jung, D. Shin, Quaternary ammonium-bearing perfluorinated polymers for anion exchange membrane applications, Membranes 10 (2020) 306, https://doi.org/10.3390/membranes10110306.
[54] M.A. Vandiver, J.L. Horan, Y. Yang, E.T. Tansey, S. Seifert, M.W. Liberatore, A. M. Herring, J. Polym. Sci., Part B: Polym. Phys. 51 (2013) 1761–1769, https://doi.org/10.1002/polb.23171.
[55] S. Bonizzoni, P. Stilli, F. Lohmann-Richters, C. Oldani, C. Ferrara, A. Papagni, L. Beverina, P. Mustarelli, Facile chemical modification of aquivion® membranes for anionic fuel cells, ChemElectroChem 8 (2021) 2231–2237, https://doi.org/10.1002/celc.202100382.
[56] F. Xu, Y. Su B. Lin, Progress of Alkaline Anion Exchange Membranes for Fuel Cells: The Effects of Micro-Phase Separation, Front. Mater., 12 February 2020 Sec. Energy Materials https://doi.org/10.3389/fmats.2020.00004.
[57] E. Passalacqua, R. Pedicini, A. Carbone, I. Gatto, F. Matera, A. Patti, A. Saccà, Effects of the chemical treatment on the physical-chemical and electrochemical properties of the commercial nafion™ nr212 membrane, Materials 13 (2020) 5254, https://doi.org/10.3390/ma13225254.
[58] S. Campagna Zignani, M. Lo Faro, A. Carbone, C. Italiano, S. Trocino, G. Monforte, A.S. Aricò, Performance and stability of a critical raw materials-free anion exchange membrane electrolysis cell, Electrochim. Acta 413 (2022), 140078, https://doi.org/10.1016/j.electacta.2022.140078.
[59] A. Carbone, S. Campagna Zignani, I. Gatto, S. Trocino, A.S. Aricò, Assessment of the FAA3-50 polymer electrolyte in combination with a NiMn2O4 anode catalyst for anion exchange membrane water electrolysis, Int. J. Hydrogen Energy 45 (2020) 9285–9292, https://doi.org/10.1016/j.ijhydene.2020.01.150.
[60] S. Petricci, P. A. Guarda, C. Oldani, G. Marchionni, Liquid compositions of fluorinated anion exchange polymers, WO 2012/098146 A1, Publication date 26-Jul-2012.
[61] E. Moukheiber, G. De Moor, L. Flandin, C. Bas, Blend membranes of polybenzimidazole and an anion exchange ionomer (FAA3) for alkaline water electrolysis: Improved alkaline stability and conductivity, J. Membr. Sci. 389 (2012) 294–304, https://doi.org/10.1016/j.memsci.2018.07.074.
[62] S. Giancola, M. Zatoń, Á. Reyes-Carmona, M. Dupont, A. Donnadio, S. Cavaliere, J. Rozière, D.J.J. Ones, Composite short side chain PFSA membranes for PEM water electrolysis, J. Membr. Sci. 570–571 (2019) 69–76, https://doi.org/10.1016/j.memsci.2018.09.063.
[63] R. Pedicini, A. Carbone, A. Saccà, I. Gatto, G. Di Marco, E. Passalacqua, Sulphonated polysulphone membranes for medium temperature in polymer electrolyte fuel cells (PEFC), Polym. Test. 27 (2008) 248–259, https://doi.org/10.1016/j.polymertesting.2007.11.002.
[64] X. Wu, W. Chen, X. Yan, G. He, J. Wang, Y. Zhang, X. Zhu, Enhancement of hydroxide conductivity by the diquaternization strategy for poly(ether ether ketone) based anion exchange membranes, J. Mater. Chem. A 2 (2014) 12222–12231, https://doi.org/10.1039/C4TA01397B.
[65] P. V. Mazinz, N. A. Kapustina, and M. R. Tarasevich, Direct Ethanol Oxidation Fuel Cell, with Anionite Membrane and Alkaline Electrolyte, Russ. J. Electrochem., 47-3 (2011) 275–281. ISSN 1023-1935.
[66] I. Gatto, A. Saccà, D. Sebastian, V. Baglio, A.S. Aricò, C. Oldani, L. Merlo, A. Carbone, Influence of ionomer content in the catalytic layer of MEAs based on aquivion® ionomer, J. Energy Chem. 35 (2019) 168–173, https://doi.org/10.3390/polym13213832.
[67] S. Andreoli, C. Oldani, V. Fiorini, S. Stagni, G. Fornasari, S. Albonetti, Superacid Aquivion® PFSA as an efficient catalyst for the gas phase dehydration of ethanol to ethylene in mild conditions, Appl. Catal., A, General 597 (2020) 117544–117553, https://doi.org/10.1016/j.apcata.2020.117544.
[68] I. Gatto, A. Saccà, V. Baglio, A.S. Aricò, C. Oldani, L. Merlo, A. Carbone, Evaluation of hot pressing parameters on the electrochemical performance of MEAs based on Aquivion® PFSA membranes, J. Energy Chem. 35 (2019) 168–173, https://doi.org/10.1016/j.jechem.2019.03.020.
[69] I. Zadok, H. Long, B. Pivovar, A. Roznowska, A. Michalak, D.R. Dekel, S. Srebnik, J. Mol. Liq. 313 (2020) 113485, https://doi.org/10.1016/j.molliq.2020.113485.
[70] T.P. Pandey, H.N. Sarode, Y. Yang, Y. Yang, K. Vezzù, V. Di Noto, S. Seifert, D. M. Knauss, M.W. Liberatore, A.M. Herring, A highly hydroxide conductive, chemically stable anion exchange membrane, poly(2,6 dimethyl 1,4 phenylene oxide)-b-Poly(vinyl benzyl trimethyl ammonium), for electrochemical applications, J. Electrochem. Soc. 163 (7) (2016) H513–H520, https://doi.org/10.1149/2.0421607jes.
[71] A.G. Divekar, A.C. Yang-Neyerlin, C.M. Antunes, D.J. Strasser, A.R. Motz, S. S. Seifert, X. Zuo, B.S. Pivovar, A.M. Herring, In-depth understanding of the CO2 limitation of air fed anion exchange membrane fuel cells, Sustainable, Energy Fuels 4 (2020) 1801–1811, https://doi.org/10.1039/c9se01212e.
[72] A. Michael Park, Z.R. Owczarczyk, L.E. Garner, A.C. Yang-Neyerlin, H. Long, C. M. Antunes, M.R. Sturgeon, M.J. Lindell, S.J. Hamrock, M. Yandrasits, Synthesis and characterization of perfluorinated anion exchange membranes, ECS Trans. 80 (2017) 957.
[73] X. Liu, H. Gao, X. Chen, Y. Hu, S. Pei, H. Li, Y. Zhang, Synthesis of perfluorinated ionomers and their anion exchange membranes, J. Memb. Sci. 515 (2016) 268–276, https://doi.org/10.1016/j.memsci.2016.05.062.
[74] M.J. Jung, C.G. Arges, V. Ramani, A perfluorinated anion exchange membrane with a 1,4-dimethylpiperazinium cation, J. Mater. Chem. 21 (2011) 6158–6160, https://doi.org/10.1039/c1jm10320b.